Theor Chem Acc (2011) 130:1131–1143
DOI 10.1007/s00214-011-1034-5

REGULAR ARTICLE

# Computational analysis of ligand recognition mechanisms by prostaglandin $E_2$ (subtype 2) and $D_2$ receptors

**Hiromi Daiyasu · Takatsugu Hirokawa · Narutoshi Kamiya · Hiroyuki Toh**

Received: 13 April 2011 / Accepted: 29 August 2011 / Published online: 20 September 2011


**Abstract** The eight members of the prostanoid receptor family belong to the class A G protein-coupled receptors. We investigated the evolutionary relationship of the eight members by a molecular phylogenetic analysis and found that prostaglandin $E_2$ receptor subtype 2 ($EP_2$) and prostaglandin $D_2$ receptor (DP) were closely related. The structures of the ligands for the two receptors are similar to each other but are distinguished by the exchanged locations of the carbonyl oxygen and the hydroxy group in the cyclopentane ring. The ligand recognition mechanisms of the receptors were examined by an integrated approach using several computational methods, such as amino acid sequence comparison, homology modeling, docking simulation, and molecular dynamics simulation. The results revealed the similar location of the ligand between the two receptors. The common carboxy group of the ligands interacts with the Arg residue on the seventh transmembrane (TM) helix, which is invariant among the prostanoid receptors. $EP_2$ uses a Ser on TM1 to recognize the carbonyl oxygen in the cyclopentane ring of the ligand. The Ser is specifically conserved within $EP_2$. On the other hand, DP uses a Lys on TM2 to recognize the hydroxy group of the $\omega$ chain of the ligand. The Lys is also specifically conserved within DP. The interaction network between the D(E)RY motif and TM6 was found in $EP_2$. However, DP lacked this network, due to the mutation in the D(E)RY motif. Based on these observations and the previously published mutational studies on the motif, the possibility of another activation mechanism that does not involve the interaction between the D(E)RY motif and TM6 will be discussed.

**Keywords** Prostanoid receptor · Prostaglandin $E_2$ · Prostaglandin $D_2$ · Ligand specificity · Molecular evolution · Molecular dynamics simulation

Dedicated to Professor Akira Imamura on the occasion of his 77th birthday and published as part of the Imamura Festschrift Issue.

**Electronic supplementary material** The online version of this article (doi:10.1007/s00214-011-1034-5) contains supplementary material, which is available to authorized users.

H. Daiyasu (✉)
The Center for Medical Engineering and Informatics, Osaka University, 1-5, Yamadaoka, Suita Osaka 565-0871, Japan
e-mail: daiyasu@ist.osaka-u.ac.jp

T. Hirokawa · H. Toh
Computational Biology Research Center, Advanced Industrial Science and Technology, 2-4-7 Aomi, Koto-ku, Tokyo 135-0064, Japan
e-mail: t-hirokawa@aist.go.jp

H. Toh
e-mail: toh-hiroyuki@aist.go.jp

N. Kamiya
Institute for Protein Research, Osaka University, 6-2-3, Furuedai, Suita Osaka 565-0874, Japan

H. Toh
Medical Institute of Bioregulation, Kyushu University, 3-1-1 Maidashi, Higashi-ku, Fukuoka 812-8582, Japan

## 1 Introduction

Stimulation of cells with proinflammatory factors activates phospholipase $A_2$, which releases arachidonic acid from the membrane phospholipids to the cytoplasm [1]. From arachidonic acid, a wide variety of bioactive compounds, such as prostaglandins (PGs), thromboxanes (TXs), leukotrienes, and lipoxins, are generated by several enzymes. The first step in the generation of PGs and TXs, which are collectively termed prostanoids, is catalyzed by

cyclooxygenase. Therefore, the prostanoid generation pathway is called the "cyclooxygenase pathway" (see Fig. 1). The prostanoids, which include $PGD_2$, $PGE_2$, $PGF_{2\alpha}$, $PGI_2$ (prostacyclin), and $TXA_2$, are involved in essential biological functions, such as inflammation, blood clotting, and sleep induction [1]. Most prostanoids function as autacoids and exert their physiological functions through binding to their own receptors on the cells. The prostanoid synthases and receptors are being extensively investigated as targets for medicines and therapeutics [2–6].

The prostanoid receptors (PNRs) belong to the class A G protein-coupled receptor (GPCR) family [6]. GPCRs are membrane proteins characterized by seven transmembrane helices (TM1–7), which are connected by three intracellular loops (ICL1–3) and three extracellular loops (ECL1–3). The alteration of the relative locations of the helices caused by ligand binding is considered to induce signal transduction. There are four $PGE_2$ receptor subtypes, which are referred to as $EP_1$–$EP_4$. In contrast, $PGD_2$, $PGF_{2\alpha}$, $PGI_2$, and $TXA_2$ uniquely correspond to their receptors, DP, FP, IP, and TP, respectively. In addition, a chemoattractant receptor-homologous molecule expressed on Th2 cells (CRTH2) was recently reported to function as a $PGD_2$ receptor [7]. Previous studies suggested that DP, $EP_1$–$EP_4$, FP, IP, and TP are closely related and form a subfamily in the class A GPCRs. However, CRTH2 is distantly related to the other PNRs, suggesting that CRTH2 may have evolved independently from the other PNRs [8].

The ligand recognition mechanism by the receptors is an important and interesting subject and is presently being analyzed experimentally and computationally. For example, the residues involved in the ligand recognition by PNRs have been experimentally investigated by amino acid substitution studies [9–13]. In addition, computational methods, such as molecular dynamics simulation [14] and homology modeling [11], have also been applied to the analysis of the ligand recognition. In this report, we describe a synergistic approach integrating several computational methods for the analysis of the ligand recognition specificity of the PNRs. At first the targets of this study were selected by a molecular phylogenetic analysis. In the phylogenetic tree $EP_2$ and DP are closely related to each other. In addition, the structures of their ligands, $PGE_2$ and $PGD_2$, are similar (see Fig. 1). The only difference between $PGE_2$ and $PGD_2$ is that the carbonyl oxygen and the hydroxy group are exchanged at positions 9 and 11 of the cyclopentane ring. Therefore, $EP_2$ and DP were selected as the targets in this analysis. Although amino acid sequence data for the receptors are abundantly available, no PNR structure has been determined yet. However, coordinate data for several class A GPCRs are available. We built the model structures of $EP_2$ and DP by homology modeling, using the structure of squid rhodopsin as a template. Sequence comparisons and model structure studies indicated the candidate residues that may be involved in the ligand specificity. Finally, molecular dynamics (MD) simulations of the ligand-bound models in

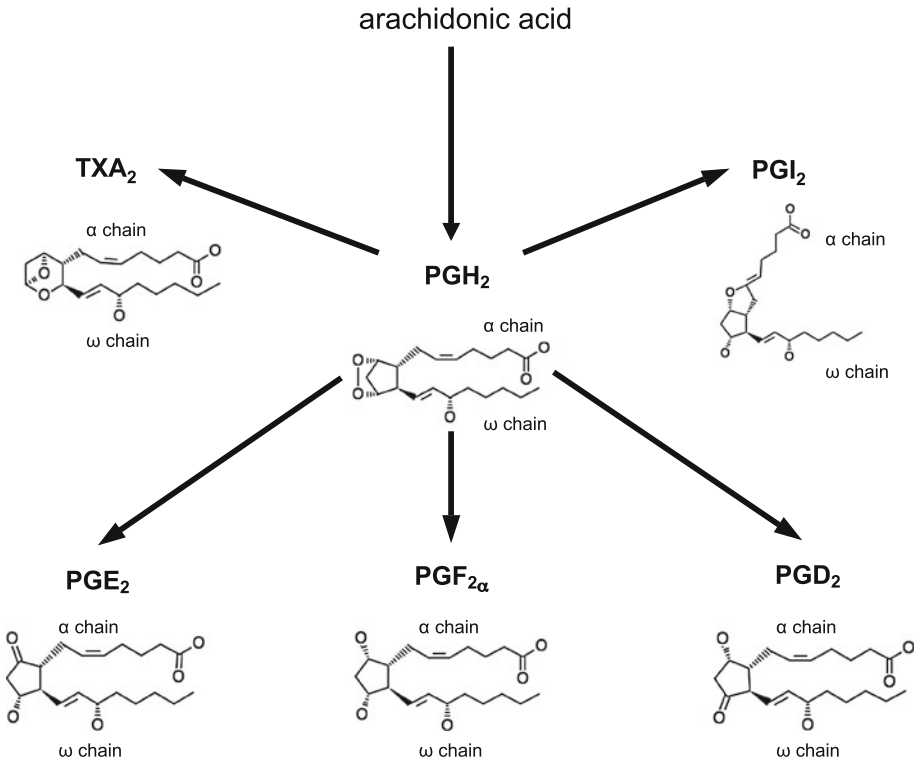


**Fig. 1** Cyclooxygenase pathway

explicit lipid and water were performed. Based on the computational results, the ligand specificities of $EP_2$ and DP will be discussed.

We will also discuss the D(E)RY motif of the PNRs. The D(E)RY motif is present at the cytosolic end of TM3, which regulates the receptor activation and the interaction with G proteins [15]. The first acidic residue, Asp or Glu, of the motif is involved in receptor activation and in coupling agonist binding to the activation of G protein signaling [16–18]. The second residue (Arg) of the motif is highly conserved and is essential for the intramolecular interactions that constrain receptors in either the inactive or activated conformation [19]. In contrast, the third residue of the motif is not highly conserved, although the Tyr residue participates in intramolecular contacts in some GPCRs that are important for stabilizing the receptor protein in a functional conformation [20]. The intramolecular interaction between the D(E)RY motif and TM6 was observed in $EP_2$, but not in DP, due to the mutation in the D(E)RY motif. Based on these observations, we will discuss the possibility that the activation mechanism through the D(E)RY motif has diverged during the course of the molecular evolution of PNRs.

## 2 Methods

### 2.1 Sequence data and representation of amino acids

The amino acid sequences of PNR homologues were collected by searching the non-redundant protein sequence database at the NCBI site (http://www.ncbi.nlm.nih.gov/BLAST/) with BLAST version 2.2.23 [21], using the human DP sequence as a query. Searches were also performed against several genome databases. Among them, one PNR homologue was detected from the genome database of *Lottia gigantea* (http://genome.jgi-psf.org/Lotgi1/Logti1.home.html). Since most mammals have all eight PNR members, the human, mouse, dog, and bovine homologues were selected as the representative mammalian PNRs in this study.

The one-letter and three-letter representations of amino acids used in this manuscript are as follows: A, Ala—alanine; C, Cys—cysteine; D, Asp—aspartic acid; E, Glu—glutamic acid; F, Phe—phenylalanine; G, Gly—glycine; H, His—histidine; I, Ile—isoleucine; K, Lys—lysine; L, Leu—leucine; M, Met—methionine; N, Asn—asparagine; P, Pro—proline; Q, Gln—glutamine; R, Arg—arginine; S, Ser—serine; T, Thr—threonine; V, Val—valine; W, Trp—tryptophan; and Y, Tyr—tyrosine.

The residues in the transmembrane region are numbered according to the Ballesteros–Weinstein nomenclature in superscript [22]. The first digit indicates the number of the TM helix on which the residue is located, and the second digit is the position counted from the most conserved site in each TM, to which number 50 is assigned. As for the residue in the loop region, the abbreviated name of the loop is shown in parentheses.

### 2.2 Phylogenetic analysis

A multiple amino acid sequence alignment was performed with the alignment software MAFFT version 6.808a [23, 24]. Based on the alignment, an unrooted molecular phylogenetic tree was constructed by the neighbor-joining (NJ) method [25]. The genetic distance between every pair of aligned sequences was calculated as a maximum likelihood estimate [26] under the JTT model [27] for the amino acid substitutions. The sites including gaps in the alignment were excluded from the calculation. The statistical significance of the NJ tree topology was evaluated by a bootstrap analysis [28]. The procedure for the bootstrap analysis is as follows: (1) Prepare a register for each node of the original tree, which is set to 0. (2) Sample the alignment sites randomly without replacement from the alignment used for the construction of the original tree. The number of collected sites should be the same as that of the original alignment. (3) Construct a phylogenetic tree with the collected alignment sites. (4) Examine each node of the tree. If the set of proteins under the node is the same as that of a node of the original tree, then one is added to the register of the node. (5) Repeat steps (3)–(4) by a given number of times. In this study, 1,000 iterations were done for the bootstrap analysis. (6) Divide the number in each register by the given number, which provides the bootstrap probability of the corresponding node. Two software packages, PHYLIP 3.5c [29] and MOLPHY 2.3b3 [30], were used for the phylogenetic analyses.

### 2.3 Construction of the model structures of $EP_2$ and DP

The amino acid sequences of proteins with available coordinates were collected by a BLAST search through the Protein Data Bank (PDB). The amino acid sequence of DP was used as a query for this search. The database search yielded squid rhodopsin, bovine rhodopsin, turkey $\beta_1$ adrenergic receptor, human $\beta_2$ adrenergic receptor, and human $A_{2A}$ adenosine receptor. The squid rhodopsin showed the lowest *E*-value in the output list (see Supplement 1). The sequence identities of the query to the five structures were only about 20%. Among them, the sequence identity between the query and the squid rhodopsin was ranked third. However, the sequence positive percent between the query and the squid rhodopsin was ranked second. Amino acid substitutions and/or a domain fusion were introduced into turkey $\beta_1$ adrenergic receptor and human $A_{2A}$ adenosine receptor, to determine the

structures. There are many unidentified regions in human $\beta_2$ adrenergic receptor due to the low-resolution analysis. However, there are no such artificial modifications in the squid and bovine rhodopsins. Considering the results of the database search, the situation of the artificial modification, and the resolution of the structure, the coordinates of the squid rhodopsin structure (pdb ID: 2Z73) were used as the template to build the model structures of $EP_2$ and DP.

A multiple alignment of DP, $EP_2$, squid rhodopsin, and the remaining four structures was created by MAFFT [23, 24]. The alignment was modified by visual inspection, so the gaps were not aligned to the secondary structure regions. In the operation, the structural information of the four structures, as well as that of the squid rhodopsin, was also considered. In general, the N- and C-terminal regions of GPCRs are divergent from each other in both length and residue composition. Therefore, the model structure was built from Q9 to L330 for $EP_2$ and from P4 to I338 for DP, respectively.

The model structures for $EP_2$ and DP were built by homology modeling with MOE (Molecular Operating Environment, version 2008.1002, Chemical Computing Group, Montreal, Canada). Energy minimization was performed with the MMFF94x force field [31], under an implicit solvent model using the generalized Born/volume integral (GB/VI) model [32]. In the model building procedure, hydrogen atoms were added to the template structure, partial charges were assigned to all of the atoms of the structure, and the dielectric constant was set to 1.0. Energy minimization was performed by the successive application of three methods, the steepest descent, the conjugate gradient, and the truncated Newton. The root mean square deviation (RMSD) gradient was set to 1,000 during the steepest descent stage and 100 in the conjugate gradient stage and was finally fixed at 0.001 in the truncated Newton stage. Then, 25 intermediate model structures were generated by the Boltzmann-weighted randomized modeling procedure, and minimizations were performed until an RMS gradient of 1 kcal/mol/Å was attained. Among them, the final model was selected based on the GB/VI scoring, which was subsequently minimized until an RMS gradient of 0.5 kcal/mol/Å was attained.

The model structures were validated by a Ramachandran plot and ProSA. The stereochemical qualities of the models were evaluated using a Ramachandran plot in MOE. The ProSA tool was used to check the overall and local structures for potential errors [33, 34]. As the baseline, validation data for the template structure were also assessed.

### 2.4 Construction of the initial ligand-bound model structures of $EP_2$ and DP

The coordinates of $PGD_2$ were obtained from the PDB (1RY0), while the 3-D structure of $PGE_2$ was constructed by modifying $PGD_2$ with MOE. Plural candidate docking models for the receptor and the ligand were generated by MOE ASEDock [35]. The ASEDock docking was performed in this study as follows: (1) generation of 1,000 ligand conformations by the stochastic conformation search, (2) concavity search of a target protein, (3) characterization of the surface and the surrounding region of the detected concavity to generate a model for ligand binding at the selected concavity, which is called an ASE model, (4) rigid body alignment of 3,000 poses for each ligand conformation to the ASE model and selection of 200 poses with the best scores to evaluate the fitness of the poses to the ASE model, and (5) stepwise energy minimization of the 200 posed conformations of the ligand in the concavity. In step (5), the ligand was free to move and the backbone atoms of the receptor were constrained by using the tether weights of the default values throughout all of the minimization procedures. In the first rough minimization, a cutoff distance of 4.5 Å and a convergence criterion for the RMS gradient of 10 kcal/mol/Å were used. The interaction energies were then calculated with a cutoff distance to 8 Å, and ten structures with the minimum interaction energies were selected. Likewise, ten structures with the maximum ASE scores were selected, although the structures that were also detected by the minimum interaction energy criterion were neglected. The structures thus selected were further refined by setting the cutoff distance to 10 Å and the RMS gradient to 0.1 kcal/mol/Å. The protein–ligand interaction energy $U_{\text{total}}$ is expressed as follows: $U_{\text{total}} = U_{\text{ele}} + U_{\text{vdw}} + U_{\text{solv}} + U_{\text{ligand}}$, in which $U_{\text{ele}}$, $U_{\text{vdw}}$, and $U_{\text{solv}}$ indicate the coulombic, van der Waals, and generalized Born/solvent accessible solvation interaction energies, respectively. $U_{\text{ligand}}$ indicates the internal conformation energy of the ligand. The obtained docking models for MD were classified based on the similarity in ligand conformation by using the cluster analysis function of ASEDock, although the models with the positive $U_{\text{total}}$ were neglected from the subsequent procedure. The members in which the carboxy group of the ligand was close to the conserved $Arg^{7.40}$ on TM7 were then collected from each cluster, since the residue is involved in the recognition of the carboxy group of the prostanoids [9–13]. Among them, the model with the lowest $U_{\text{total}}$ was selected as the representative of the cluster. Finally, the model structure with the lowest $U_{\text{total}}$ among the representatives of the clusters was selected as the initial ligand-bound model structure for the following MD simulations.

### 2.5 MD simulations

Molecular dynamics simulations of the ligand-bound forms, built as described above, were performed for both

$EP_2$ and DP using Desmond version 2.2 [36]. The OPLS2005 force field [37] was used for the simulations. Initial ligand-bound model structures were placed into a large equilibrated dipalmitoylphosphatidylcholine (DPPC at 325 K) bilayer and TIP3P water molecules solvated with 0.15 M NaCl. The resulting system for the ligand-bound $EP_2$ had 179 lipid molecules, 48 sodium ions, 48 chloride ions, and 17,396 water molecules, for a total of 80,754 atoms, and the boundary condition measured $\approx 89 \times 83 \times 118$ Å$^3$. The resulting system for the ligand-bound DP had 171 lipid molecules, 55 sodium ions, 55 chloride ions, and 19,618 water molecules, for a total of 86,582 atoms, and the boundary condition measured $\approx 90 \times 82 \times 127$ Å$^3$. All system setups were performed using Maestro (Schrödinger LLC, New York NY). No artificial constraint was introduced in the simulation. After minimization, heating, and equilibration, the production MD phase was performed for 10 ns in the isothermal-isobaric (NPT) ensemble at 310 K and 1 bar using the Berendsen coupling scheme. The covalent bonds involving hydrogen atoms were constrained by the M-SHAKE method [38]. The time step of the MD was 2 fs. The van der Waals and short-range electrostatic interactions were truncated with a 9-Å-cutoff. Long-range electrostatic interactions were computed using the Particle Mesh Ewald method [39].

The equilibrium of the MD simulation was evaluated by the RMSDs between the Cα atoms of the model structure at each time step of a run and those of the reference structure. Here, the first structure (0 ns) in the production MD phase was used as the reference structure. The total potential energy was also used to evaluate the equilibrium, which was calculated by summing up the energies of bond stretching, angle bending, and torsional potential, their cross terms, and the non-bonded interaction energies (van der Waals and coulomb) for all systems including a protein with ligand, lipids, ions, and water molecules. The fluctuation of each Cα atom of the model structures in the equilibrium state was evaluated with the root mean square fluctuation (RMSF). The trace in a time window of 10 ns in the equilibrium state was obtained from each run of the simulation, and then the average coordinates over the window were calculated. The squared deviation of each Cα atom between the model structure and the average coordinates was averaged over the 10 ns. The square root of the averaged value of an atom was the RMSF for the atom. The interaction energy for a ligand–receptor complex was calculated by the Prime MM-GBSA [40] in Maestro using 10 MD conformations, corresponding to each 0.1-ns step of the final 1-ns trajectories.

## 3 Results

### 3.1 Molecular evolution of PNRs

#### *3.1.1 Phylogenetic analysis of PNRs*

To examine the evolutionary relationships of PNRs, the sequences of PNR homologues and several class A GPCR proteins were collected and aligned (Supplement 2). A phylogenetic tree of these proteins is shown in Fig. 2. The tree is divided into two subtrees, which are rooted at nodes X and Y, respectively. One of them consists of four PNR clusters, corresponding to $EP_4$, IP, $EP_2$, and DP, whereas the remaining four PNR clusters, $EP_3$, TP, FP, and $EP_1$, constitute the other subtree. Both subtrees included different subtypes of $PGE_2$ receptors. The distribution of PNRs in the tree suggests that the current receptors originated from an ancestral receptor for $PGE_2$, consistent with previous reports [8, 41]. Each PNR cluster includes the putative vertebrate orthologues, which suggests that the genome of an ancestral organism of vertebrates already encoded the eight PNRs. The amphioxus (*Branchiostoma floridae*) and the ascidian (*Ciona intestinalis*), which are close relatives of vertebrates, had one or two copies of PNR homologues. The vertebrates, the amphioxus, and the ascidian constitute the deuterostome. PNR homologues were also found in the mollusk (*L. gigantea*), which belongs to the protostome. Currently, the genome data for several protostomes, such as insects and nematoda, are available. However, PNR homologues were not detected in the genome data of these organisms. On the other hand, a PNR homologue was also detected from the cnidarian (*Nematostella vectensis*). The cnidarian is considered to have branched out before the divergence of the protostome and the deuterostome. The vertebrate PNRs have a conserved $Arg^{7.40}$ on TM7, which is believed to be essential to interact with the carboxy group of prostanoids [9–13]. This residue does not exist in the other class A GPCRs. The $Arg^{7.40}$ residue was also conserved in the invertebrate PNR homologues, except for those from *C. intestinalis* (gi number: 198418121) and *B. floridae* (gi number: 260823840) (see Supplement 2). The tree topology, together with the conservation of the Arg residue, suggests the possibility that the date for the divergence between the two subtrees would trace back before the divergence between the protostome and the deuterostome. Further accumulation of genome data will reveal the cause of this bias in the distribution of PNR homologues.

One of the interesting points of the tree was the close evolutionary relationship between $EP_2$ and DP. The bootstrap probability for the clustering of the two receptors was 89.9%, and the sequence identity between the two

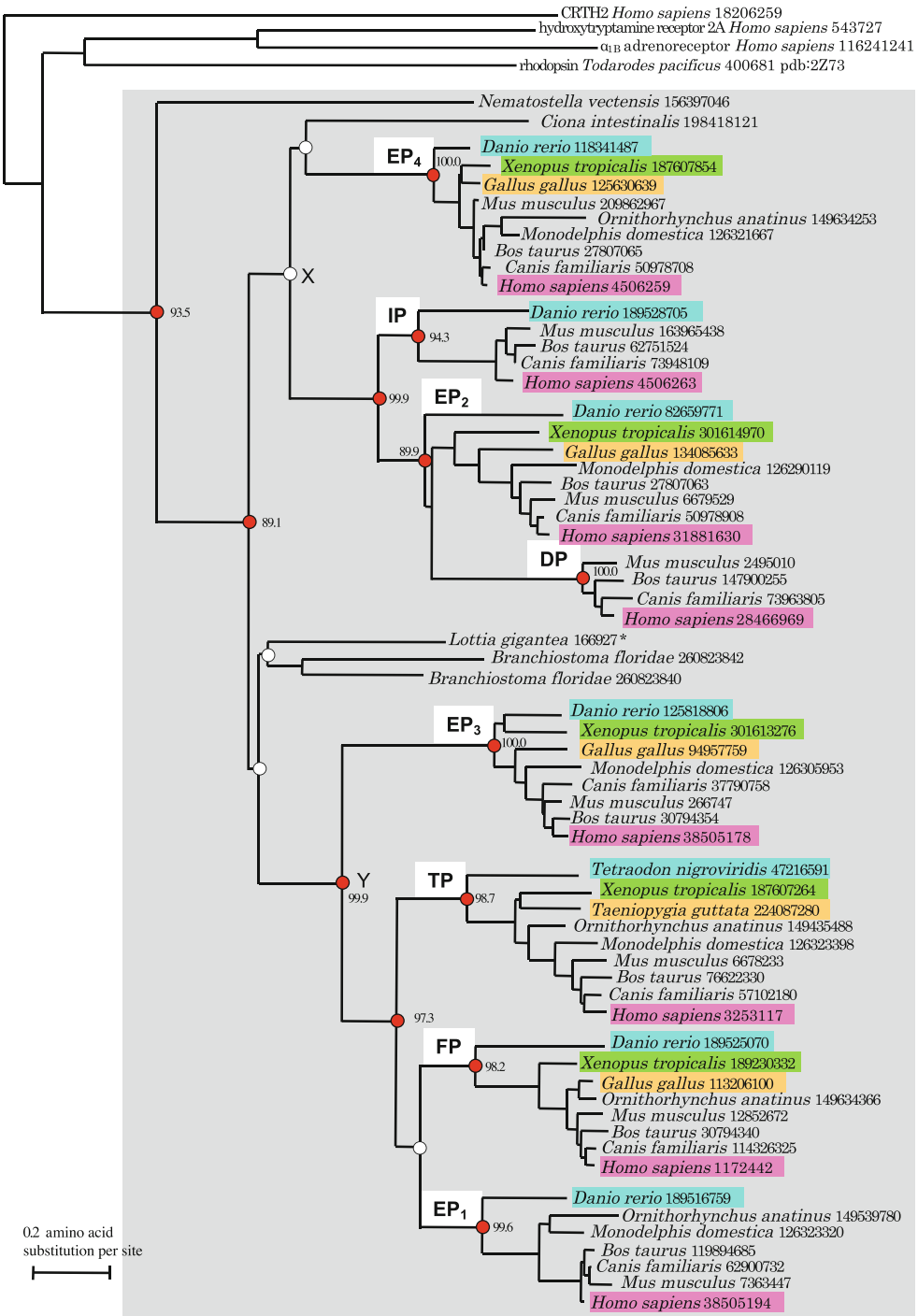


**Fig. 2** Phylogenetic tree of PNRs. PGR homologues are within the *gray rectangle*. The other class A GPCRs outside the *rectangle* are introduced as the outgroup. The source organism and the NCBI gi number for each sequence are shown at the terminal node. *Asterisk* indicates the sequence derived from *L. gigantea* genome data (see Sect. 2). The nodes that are considered to be critical for the evolution of the PNRs are indicated by *circles*. Critical nodes with bootstrap probabilities >80% are colored *red*, with the bootstrap probability shown near the node

receptors was about 40%. As described above, the structures of the ligands for the two receptors are quite similar to each other. The only difference is that the positions of the carbonyl oxygen and the hydroxy group are exchanged in the cyclopentane ring (Fig. 1). Thus, the structural similarity of the ligands seems to reflect the evolutionary closeness of the receptors. The medium sequence divergence of the receptors and the resemblance of the ligand structures made it challenging to investigate the relationship between the differences in the amino acid residues and the ligand recognition specificity of the receptors. In this study, we have analyzed the mechanism of the ligand recognition specificity by focusing on $EP_2$ and DP.

### 3.1.2 *Conservation pattern of amino acid residues in PNRs*

At first, we examined the residue conservation by constructing a multiple alignment of PNRs (Supplement 2).

We obtained 24 invariant sites among all of the PNR homologues, which are shown in the alignment of $EP_2$ and DP (Fig. 3). The invariant $Arg^{7.40}$ was also included in these sites. Some of the sites may also be involved in the recognition of the common structure of prostanoids, such as $Arg^{7.40}$. The conserved sites also included the NPxxY motif on TM7, although the motif was found as DPWxF in the PNRs. This motif contributes to the internalization and the signal transduction of class A GPCRs [42]. The cholesterol-binding motif on TM4 [43] was not found in the PNRs.

Next, we examined the amino acid conservation pattern between $EP_2$ and DP (Fig. 3). We assumed that the amino acid sites specifically conserved in $EP_2$ or DP are involved in the specific ligand recognition by the receptors. Thus, the sites that are invariant in $EP_2$, but are not occupied by the same residue in DP, were identified from the alignment at first. The DP-specific invariant sites were identified in the same manner. We identified 21 sites for $EP_2$ and 76 for DP. Hereafter, these residues will be referred to as "specifically conserved sites". The abundance of the specifically conserved residues in DP, in comparison with $EP_2$, was considered to reflect the difference in the evolutionary closeness of the sources, since the amino acid sequences of DP were only from mammals, whereas the sequences of $EP_2$ used in this study were collected from vertebrates. As described below, the candidate sites involved in the ligand recognition were further selected from these specifically conserved sites, considering the structural information of the model structures.

In addition to the specifically conserved sites, we identified 164 alignment sites that are occupied by physicochemically similar residues between $EP_2$ and DP. These sites will simply be called "conserved sites". Naturally, the 24 invariant sites within PNRs described above were included in the sites. Most of the 164 conserved sites were found in the seven TM helices, based on the model structures, as described below. Some of the conserved sites were found in ICL2 and ECL2. The observation suggests that the conservation may reflect the common structural and/or functional constraints on the receptors. Therefore, the residues corresponding to the conserved sites were also regarded as the candidate residues involved in the ligand recognition.

## 3.2 Molecular mechanisms of ligand recognition by $EP_2$ and DP

### 3.2.1 *Model construction of $EP_2$ and DP*

The ligand-free models for $EP_2$ and DP were constructed by homology modeling, as described in Sect. 2. To assess

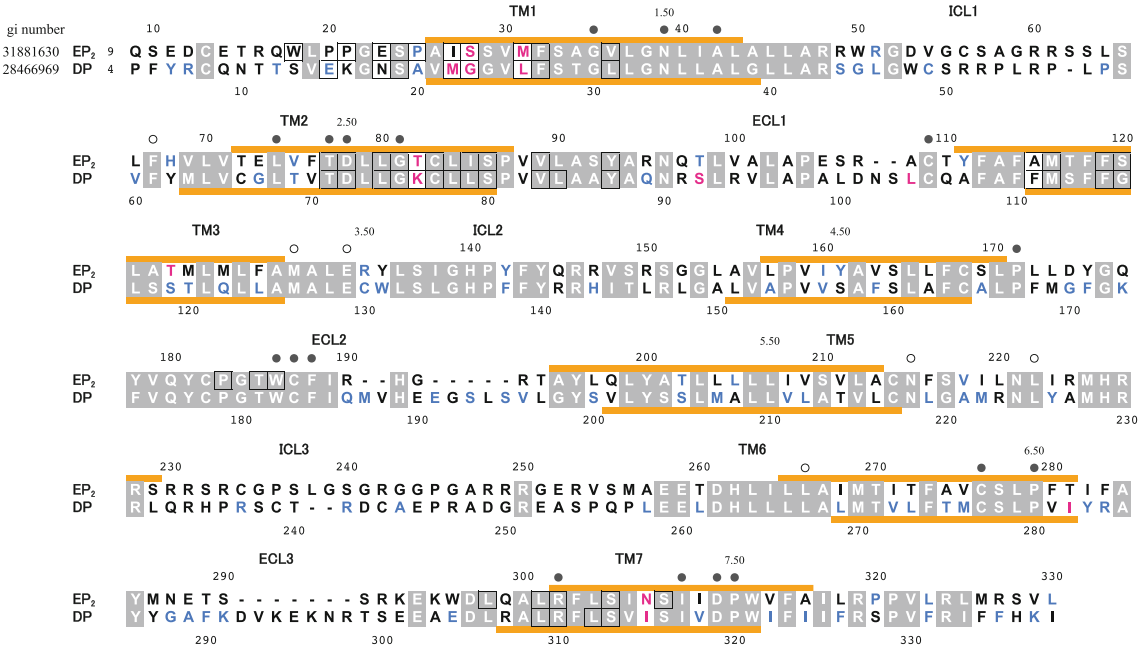


**Fig. 3** Amino acid sequence alignment of human $EP_2$ and DP. Among the sites specifically conserved in each subfamily, those located in the pocket surface regions detected by CASTp [44] are colored *red*, whereas the remaining sites are colored *blue*. The conserved sites between $EP_2$ and DP are represented by *white* characters with a *gray* background. The invariant sites among the PNR homologues are indicated by the *circles* over the alignment (*black*: located in the ligand-binding pocket, *white*: near the D(E)RY motif). The *orange bar* shows the TM regions predicted by TMDET [52]. For the prediction, the model structure with the lowest MM-GBSA energies was used. The residues located within 5 Å from the ligand were obtained from the selected model structures, which are *encircled* by *black squares* in the alignment

the quality of the structures, the generated models were examined by the Ramachandran plots and the ProSA program (Supplement 3). One residue for $EP_2$ and eight for DP were identified as outliers in their phi and psi backbone dihedral angles by the Ramachandran plot evaluation. All residues thus identified were located in loop regions and were far from the pocket and the D(E)RY motif. The ratios of the residues of the model structures in the core region were 93.4% for $EP_2$ and 87.7% for DP. The ProSA program evaluates a model structure by two methods. One of them is the overall model quality in comparison with the experimentally determined structural data in the PDB database, and the goodness of the model by this evaluation is given by the *Z*-score. The *Z*-score for the $EP_2$ model structure was −5.84 and that for the DP model structure was −6.13, whereas the *Z*-score of the template structure was −4.94 (see Supplement 3). In the other method, the local model quality is expressed as a function of the amino acid sequence position. In general, an amino acid segment with positive values indicates erroneous parts of the given structure. There were far fewer such regions in the $EP_2$ and DP model structures than in the template. Thus, both evaluations suggested that the model structures were built with good quality. Therefore, we used the model structures to build the models of the ligand-bound forms of $EP_2$ and DP.

The candidate residues involved in the ligand recognition were selected from the residues corresponding to the specifically conserved sites described above. At first, the cavity of each model structure was identified by CASTp [44], a program to identify the surface accessible pockets of a given tertiary structure. Then, the residues corresponding to the specifically conserved sites, which were located on the surface of the detected cavity, were selected as the candidates. Five residues were selected for $EP_2$, while eight specifically conserved residues were found in the cavity of DP. These residues are shown in Fig. 3.

ASEDock generated 16 ligand-bound models for $EP_2$ and 20 ligand-bound models for DP (see Supplement 4). Among the 16 $EP_2$ models, 10 models with negative $U_{total}$ were selected and classified into five groups by the cluster analysis. According to the procedure described in Sect. 2, the representative model of group 1 with $U_{total}$ of −35.5 kcal/mol was selected as an initial model structure for the MD simulation. The distance between the oxygen in the carboxy group of the ligand and the hydrogen in the guanidino group of $R302^{7.40}$ for $EP_2$ was 2.0 Å. Likewise, 18 ligand-bound models for DP with negative $U_{total}$ were selected from the 20 models and classified into seven groups. The selection procedure chose the representative model of group 2 with $U_{total}$ of −59.5 kcal/mol as the initial structure for the MD simulation. The distance between the ligand and $R310^{7.40}$ of DP was 1.7 Å. To identify the residues that can stably interact with the ligand, the ligand-bound models for $EP_2$ and DP were subjected to the MD simulation.

### 3.2.2 *MD simulations of $EP_2$ and DP*

Molecular dynamics simulations were monitored with the RMSD and the potential energy, as described in Sect. 2. Supplement 5 shows a plot of the RMSD between each model structure during the MD trajectory and the initial model structure. In each model system, the RMSD reached equilibrium and oscillated around the average value after 4–5 ns. The potential energies for the entire systems during the MD trajectory are shown in Supplement 6. The energies rapidly reached equilibrium for both systems with the $EP_2$ and DP models.

As described above, the conserved $Arg^{7.40}$ of PNRs is considered to interact with the carboxy group of prostanoids [9–13]. The length of the salt bridge between the carboxy group and the Arg was monitored during the simulation (Supplement 7) and suggested that the interaction was stable in ligand-bound models of both $EP_2$ and DP.

To evaluate the fluctuation of each residue of the model systems during MD, the RMSF was calculated for the Cα atom. The RMSF is plotted as a function of the residue position in Supplement 8. As shown in the plots, the fluctuations of the TM helices in both the $EP_2$ and DP model structures were small. In contrast to those regions, the fluctuations of the loop regions were large. Especially, the N-terminal loop, ICL1, and ICL3 of the $EP_2$ model structure greatly fluctuated, whereas the fluctuations of the N-terminal loop and ICL3 of the DP model structure were large. ICL3 is considered to be intrinsically disordered and involved in interactions with G proteins [45]. Thus, the fluctuation in ICL3 may be related to the signal transduction by PNRs. The N- and the C-terminal loops were also suggested to be intrinsically disordered [45]. However, the fluctuations of the C-terminal loops of both PNRs were smaller than those of the other intrinsically disordered loops.

### 3.2.3 *Differences in ligand recognition mechanisms between $EP_2$ and DP*

*3.2.3.1 Interaction between $EP_2$ and $PGE_2$* As described in Sect. 2, 10 structures were sampled from the last 1 ns of the simulation of the ligand-bound model of $EP_2$. The MM-GBSA ligand interaction energies of these structures are shown in Supplement 9. The whole structure and the vicinity of the ligand in the model with the lowest MM-GBSA energy are depicted in Fig. 4. As shown in Fig. 3, 32 amino acid residues of $EP_2$ were found within 5 Å from

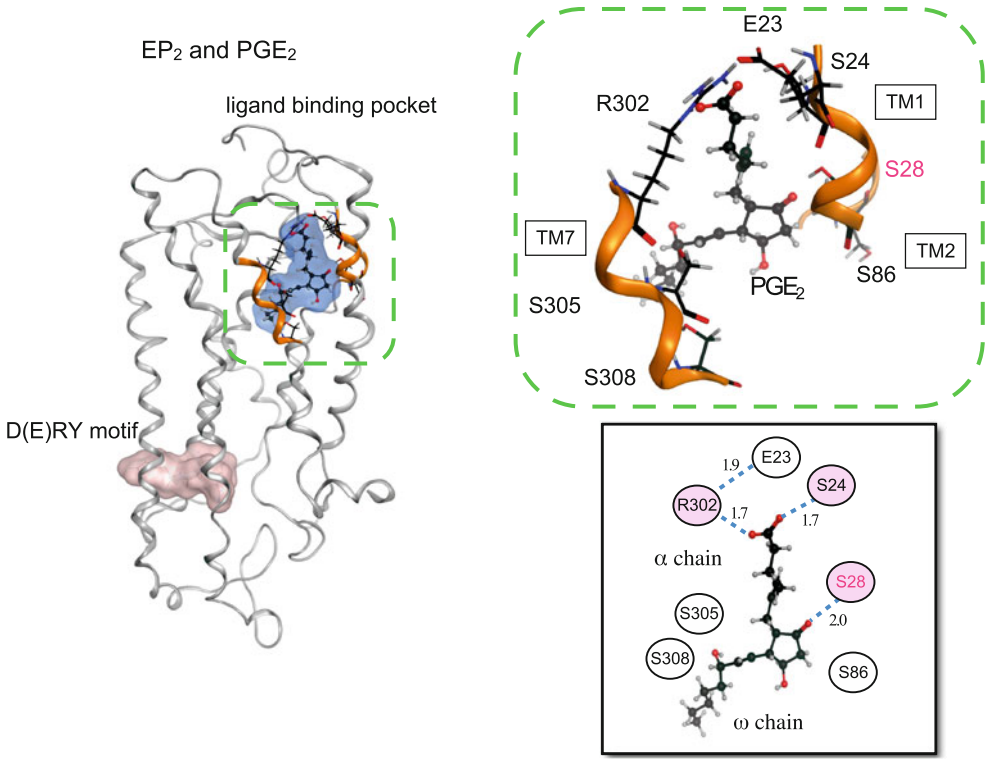


**Fig. 4** Model structure of $EP_2$ with $PGE_2$. The whole and the local structures of $EP_2$ with $PGE_2$ are shown. The schematic diagram of the ligand–receptor interaction is also shown as an *inset*, where the average distances over the MD simulation (5–10 ns) between the ligand and the residues and those between the contact residue pairs are shown

$PGE_2$. These residues were mainly located on TM1, TM2, TM3, TM7, and ECL2. The side-chain of W186 (ECL2) and that of $Y93^{2.65}$ at the end of TM2 were directed toward the ligand-binding pocket, which may determine the ligand location. The cyclopentane ring of $PGE_2$ was surrounded by four Ser residues (Fig. 4). One of them, $S28^{1.39}$, is specifically conserved in $EP_2$ and formed a stable hydrogen bond with the carbonyl oxygen of the cyclopentane ring (see Supplement 7). The remaining three Ser residues did not directly interact with $PGE_2$. $S86^{2.58}$ existed near $S28^{1.39}$. This Ser was conserved not only within $EP_2$ but also within DP. The other two Ser residues, $S305^{7.43}$ and $S308^{7.46}$, existed on the opposite side of the cyclopentane ring against $S28^{1.39}$ and $S86^{2.58}$. The two residues were also conserved in both $EP_2$ and DP. The α chain of $PGE_2$ was extended toward the extracellular region. The hydrophobic environment around the α chain comprised $I27^{1.38}$, $M31^{1.42}$, $V89^{2.61}$, $Y93^{2.65}$, W186 (ECL2), and $L301^{7.39}$. The carboxy group at the terminus of the α chain interacted mainly with $R302^{7.40}$, as described above. In addition, $S24^{1.35}$ also interacted with the carboxy group. $R302^{7.40}$ constituted a network by forming salt bridges with $E23^{1.34}$. The network may contribute to determining both the relative arrangement of TM1 and TM7 and the location of the carboxy group of $PGE_2$ in the ligand-binding pocket. On the other hand, the ω chain was extended toward the middle of the membrane. The hydrophobic environment around the ω chain was composed of $L80^{2.52}$, $I85^{2.57}$, $M116^{3.32}$, $F119^{3.35}$, and W186 (ECL2). In the model structure, no amino acid residue that directly interacts with the hydroxy group in the ω chain was observed.

From the results of the sequence comparison and the analysis with CASTp, $EP_2$ had five specifically conserved residues, $S28^{1.39}$, $M31^{1.42}$, $T82^{2.54}$, $T123^{3.39}$, and $N307^{7.45}$, on the pocket surface. The MD simulation revealed the interaction between $S28^{1.39}$ and the carbonyl oxygen in the cyclopentane ring of $PGE_2$. In DP, the corresponding site was occupied by Gly, which is not expected to be involved in ligand recognition. However, three other $PGE_2$ receptors, $EP_1$, $EP_3$, and $EP_4$, have Pro at the corresponding site. On the other hand, no interaction was observed between the ligand and $M31^{1.42}$ or $T82^{2.54}$, although they were located close to $PGE_2$. $T123^{3.39}$ and $N307^{7.45}$ were farther from to the ligand. Therefore, the four specifically conserved residues are considered to be involved in some $EP_2$-specific function other than ligand recognition. In summary, several residues on TM1, TM2, and TM7 mainly contribute to the interaction with the ligand. Among them, $S28^{1.39}$, which may be involved in $PGE_2$-specific recognition, is located on TM1 of $EP_2$.

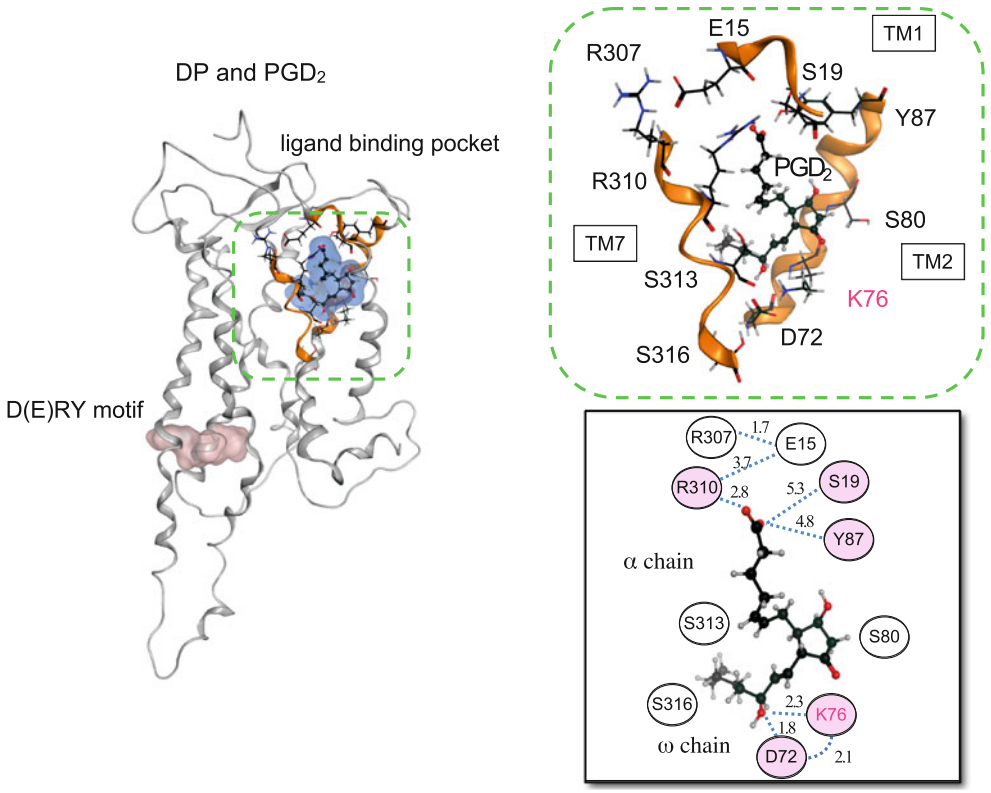


**Fig. 5** Model structure of DP with $PGD_2$. The whole and the local structures of DP with $PGD_2$ are shown. The schematic diagram of the ligand–receptor interaction is also shown as an *inset*, where the average distances over the MD simulation (5–10 ns) between the ligand and the residues and those between the contact residue pairs are shown

*3.2.3.2 Interaction between DP and $PGD_2$* As in the case of $EP_2$, 10 structures were sampled from the last 1 ns of the simulation of the ligand-bound model of DP. The MM-GBSA ligand interaction energies of these structures are shown in Supplement 9. In the DP model structure with the lowest MM-GBSA energy, 28 amino acid residues were found within 5 Å from $PGD_2$ (see Fig. 3). These residues were mainly located on TM1, TM2, TM3, and TM7. The ligand location seemed to be restricted by the bulky side chains of $Y87^{2.65}$, $F111^{3.31}$, $F115^{3.35}$, and W182 (ECL2). The whole structure and the vicinity of the ligand in the model with the lowest MM-GBSA energy are shown in Fig. 5. The hydrogen bonds between DP and $PGD_2$ described below were stable during the MD simulation (Supplement 7). The α chain was extended to the extracellular region, in a similar manner to those of $PGE_2$ in $EP_2$, and was surrounded by the hydrophobic residues $M22^{1.38}$, $L26^{1.42}$, $V83^{2.61}$, $L84^{2.62}$, $Y87^{2.65}$, $L306^{7.36}$, $L309^{7.39}$, and $V314^{7.44}$. The carboxy group at the terminus of the α chain interacted with $R310^{7.40}$. In addition, the carboxy group formed a hydrogen bond with $S19^{1.35}$ and $Y87^{2.65}$. $R307^{7.37}$ and $R310^{7.40}$ created an intramolecular salt bridge network with $E15^{1.31}$. As in the case of the ligand-bound $EP_2$ model structure, both the relative arrangement of TM1 and TM7 and the location of the carboxy group of $PGD_2$ in the ligand-binding pocket seemed to be determined by the intramolecular network. On the other hand, the ω chain was bent in the membrane and was surrounded by the hydrophobic residues, $L79^{2.57}$, $V83^{2.61}$, $F111^{3.31}$, $M112^{3.32}$, $F115^{3.35}$, $L117^{3.35}$, W182 (ECL2), $V281^{6.51}$, $L309^{7.39}$, $L312^{7.42}$, and $I315^{7.45}$. The hydroxy group in the ω chain interacted with $D72^{2.50}$ and $K76^{2.54}$, and these two residues also formed a salt bridge with each other (Supplement 7). No residue that interacted with the cyclopentane ring part was found during the simulation. Three Ser residues, $S80^{2.58}$, $S313^{7.43}$, and $S316^{7.46}$, were present in the middle of the membrane. $S313^{7.43}$ and $S316^{7.46}$ interacted with $K76^{2.54}$ (data not shown). These residues may contribute to the stabilization of the three oxygens of the cyclopentane ring and the ω chain by providing a hydrophilic environment, although there was no direct interaction between the serine residues and the oxygens. The three residues corresponded to the conserved Ser residues of $EP_2$, $S86^{2.58}$, $S305^{7.43}$, and $S308^{7.46}$.

According to the sequence comparison and the analysis with CASTp, eight residues were specifically conserved on the pocket surface in DP. Among them, $K76^{2.54}$ formed a

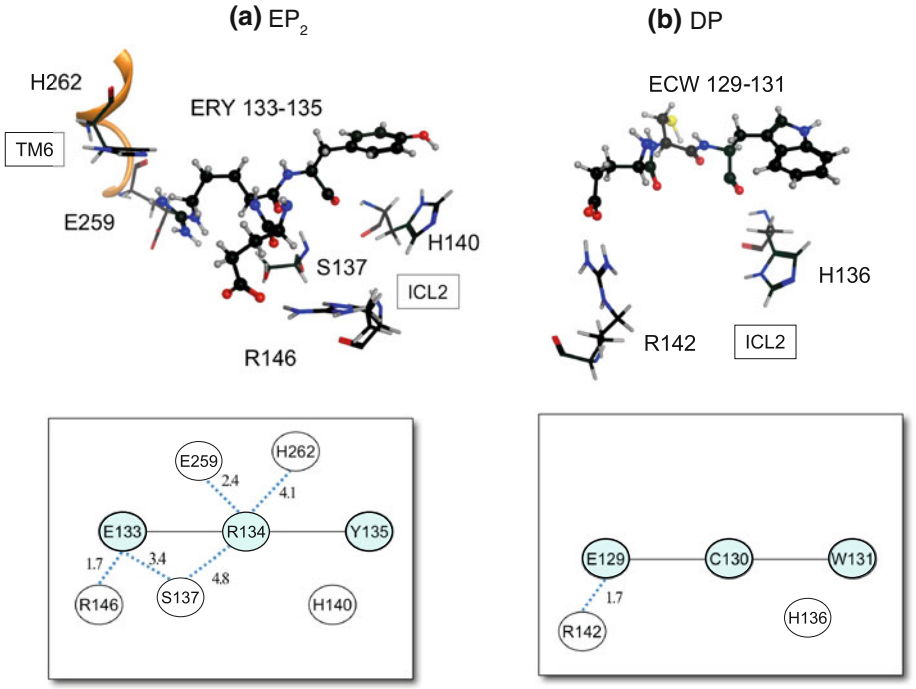


**Fig. 6** The intramolecular interaction networks around the D(E)RY motif. The structures and the schematic diagrams for (**a**) $EP_2$ with $PGE_2$ and (**b**) DP with $PGD_2$ are shown. The average distances over the MD simulations (5–10 ns) between the contact residue pairs are shown in the schematic diagram

hydrogen bond with the hydroxy group in the $\omega$ chain. The Lys was experimentally suggested to be essential for ligand recognition [46]. On the one hand, a hydrogen bond between the Lys and the carbonyl oxygen of the cyclopentane ring was formed by an MD simulation [14]. However, in our simulation, this interaction was not observed. In $EP_2$, the corresponding site was occupied by the specifically conserved $T82^{2.54}$. This Thr did not interact with the ligand in the $EP_2$ model structure. Three other specifically conserved residues, $M22^{1.38}$, $G23^{1.39}$, and $L26^{1.42}$, were found near the ligand. $M22^{1.38}$ and $G23^{1.39}$ existed near the $\alpha$ chain, whereas $L26^{1.42}$ was close to the cyclopentane ring. However, the three residues did not interact with the ligand. The remaining four residues, S92 (ECL1), L104 (ECL1), $I282^{6.52}$, and $I315^{7.45}$, were not considered to be involved in the ligand recognition, since they were farther away from the ligand. As in the case of $EP_2$, TM1, TM2, and TM7 are also important for ligand recognition in DP. In contrast to the case of $EP_2$, $K76^{2.54}$ on TM2 may be involved in the ligand recognition.

### 3.3 Differences in intramolecular interactions around the D(E)RY motif between $EP_2$ and DP

As described above, the D(E)RY motif of GPCR is important for signal transduction [15]. The vicinity around the motif, Glu–Arg–Tyr (133–135), of the $EP_2$ model structure, is shown in Fig. 6a. $E133^{3.49}$ mainly interacted with R146 (ICL2) by forming a stable salt bridge and occasionally formed a hydrogen bond with S137 (ICL2). $R134^{3.50}$ formed a stable interaction with $E259^{6.40}$ and sometimes interacted with S137 (ICL2) during the MD (Supplement 7). $R134^{3.50}$ and $H262^{6.43}$ were located close to each other and may form a $\pi$-$\pi$ interaction. The side chains of $E133^{3.49}$ and $R134^{3.50}$ were oriented in different directions, since they interact with other residues. H140 (ICL2) was present in the vicinity of $Y135^{3.51}$, the third residue of the motif. The side chains of the two residues were stacked upon one another, and the distance between them was about 5 Å. Therefore, the residues seemed to form a $\pi$–$\pi$ interaction.

As described above, the D(E)RY motif of DP is mutated to Glu–Cys–Trp (129-131). The pattern of the intramolecular network around the motif in DP was quite different from that in $EP_2$. The interaction was only detected between $E129^{3.49}$ and R142 (ICL2) (Fig. 6b). The middle residue of the motif, $R134^{3.50}$ of $EP_2$, was substituted with Cys in DP. Due to the mutation, the interaction between the motif and TM6 was not observed in the DP model structure. H136 (ICL2), which corresponded to H140 (ICL2) of $EP_2$, was present near $W131^{3.51}$. The side chains were stacked upon one another, with a distance of about 6 Å.

## 4 Discussion

In this study, we have assumed that the amino acid residues specifically conserved in $EP_2$ and DP are related to the ligand recognition by the receptors. Our simulation study suggested that one of the specifically conserved residues in $EP_2$, $S28^{1.39}$, is involved in the recognition of the carbonyl oxygen of the cyclopentane ring. However, three other

$PGE_2$ receptors, $EP_1$, $EP_3$, and $EP_4$, have Pro at the corresponding site. As described above, the ancestor of the PNRs was considered to be the $PGE_2$ receptor. The observation of Pro in $EP_1$, $EP_3$, and $EP_4$ at the site suggests that the original residue in the ancestral $PGE_2$ receptor was Pro and that the ligand recognition mechanism of $EP_2$ may be different from those of the other $PGE_2$ receptors and the ancestral receptor, although they share $PGE_2$ as their ligand. DP lacks binding affinity to $PGE_2$ [47]. In DP, the residue corresponding to $S28^{1.39}$ is substituted with Gly. Our simulation study of DP suggested that the Gly residue is not involved in the recognition of $PGD_2$. Kobayashi et al. [46] generated a chimera between IP and DP, in which ICL1, TM2, and ECL1 were derived from IP to the remaining parts of the molecule were from DP. The chimera did not bind to either $PGE_2$ or $PGD_2$. When the Gly on TM1 in the DP region of the chimera was substituted with Ser, the mutant acquired the ability to bind $PGE_2$. The experiment seems to indirectly support the importance of the Ser residue for the recognition of $PGE_2$.

On the other hand, $K76^{2.54}$ was specifically conserved in DP. Our simulation study suggested that this residue is involved in the recognition of the hydroxy group of the $\omega$ chain of $PGD_2$. No residues interacted with either the hydroxy group or the carbonyl oxygen of the cyclopentane ring of $PGD_2$ in our simulation. In contrast, no residue that could interact with the hydroxy group of the $\omega$ chain of $PGE_2$ was detected in the simulation of $EP_2$. Therefore, the hydrogen bond formation between the hydroxy group and $K76^{2.54}$ may regulate the specific ligand recognition by DP. As described above, Li et al. [14] suggested that the Lys can form a hydrogen bond with the carbonyl oxygen in the cyclopentane ring of $PGD_2$, based on their MD simulation. Thus, our result is inconsistent with their report. However, the average distance between $K76^{2.54}$ and the carbonyl oxygen was 4.9 Å, and some rotamers of the residue were in a position that could interact with the oxygen (data not shown). Therefore, it is still possible that $K76^{2.54}$ also interacts with the carbonyl oxygen. For both $PGE_2$ and $PGD_2$, the $\alpha$ chain extended toward the outside of the receptors, whereas the cyclopentane ring and the $\omega$ chain extended between TM1 and TM2. The modification of the amino acid residues on the two helices is considered to have been effective to change the ligand recognition mechanism.

The D(E)RY motif is a conserved amino acid stretch in the cytoplasmic region of TM3. The cytoplasmic interaction network between the D(E)RY motif and TM6 is considered to be involved in the activation of the receptor. The network is called an "ionic lock", which is disrupted during the activation to release the constraints on the relative movement of TM3 and TM6 in some class A GPCRs, such as rhodpsin and $\beta_2$-adrenergic receptor [48]. The salt bridge between the first and second residues of the motif in the inactivated form is also observed [15]. $EP_2$ has the canonical D(E)RY motif. $E133^{3.49}$ of the motif did not form a salt bridge with the second residue of the motif, $R134^{3.50}$, but interacted with R146 (ICL2). $R134^{3.50}$ formed a salt bridge with $E259^{6.30}$. To examine the release of the ionic lock by the simulation study, more time steps may be required. In contrast to the canonical motif of $EP_2$, the D(E)RY motif of DP is mutated. The highly conserved Arg at the second position of the motif is substituted with Cys. Rosenkilde et al. [19] examined 365 human rhodopsin-like GPCRs and reported that only 3% lack the basic residue at this position. In our simulation study, the interaction between the motif and TM6 was absent in DP, due to the mutation. However, DP can exert its signal transduction activity. Therefore, DP may use a different mechanism for receptor activation, corresponding to the ionic lock. This hypothesis seemed to be consistent with the results of the experimental studies on other class A GPCRs. The D(E)RY motifs of various GPCRs have been subjected to amino acid substitution experiments to examine their functional meanings [49]. Such mutants are expected to be constitutively active, since they cannot form the ionic lock. Actually, some GPCR mutants are constitutively active. For example, FP becomes constitutively active by the mutation of the D(E)RY motif [50]. However, quite a few mutants are not constitutively active, such as the mutant of TP [51]. Both FP and TP have the canonical D(E)RY motif. As shown in Fig. 2, $EP_2$ and DP belong to one of the subtrees, whereas FP and TP are members of the other subtree. Therefore, it seems that the activation mechanism of PNRs may have rapidly diverged during evolution, and at least DP and TP acquired the activation mechanism without the ionic lock. Further experimental and computational studies are needed to solve this problem.

We have described a synergistic study integrating different computational approaches. The evolutionary information obtained from sequence comparisons is useful to select proper targets for computational studies and to identify the candidates of functionally important residues. Structural information obtained from homology modeling and docking analyses provides further clues to refine the candidate residues. Molecular dynamics simulations provided dynamic views for this study, which could not be obtained from static analyses with sequence comparisons and modeling. Thus, combining the information obtained from different computational approaches with that from the literature seems to be more efficient than using an individual approach, if the proper combination is adopted.

In this study, we used the PNRs as a concrete example for the application of the synergistic study. However, many questions about the PNRs still remain. For example, CRTH2 is known to function as a $PGD_2$ receptor [7], but

the evolutionary origin of the receptor differs from that of DP [8], as described above. Whether CRTH2 and DP share the same ligand recognition mechanism is an interesting subject, not only from a pharmaceutical viewpoint but also from an evolutionary perspective. A synergistic study may provide clues to address this issue. Computational analyses will accelerate the studies of PNRs.

**Acknowledgments** We thank Drs. Wataru Nemoto, Kentaro Tomii, and Makiko Suwa of CBRC for useful discussions on this work. HD was supported in part by the Global COE program, "an In Silico Medicine", at Osaka University and Grants-in-Aid (Nos. 20650012 and 19650072) from the Ministry of Education, Culture, Sports, Science and Technology of Japan. HT was partially supported by Targeted Proteins Research Program (TPRP).

## References

1. Funk CD (2001) Science 294:1871–1875
2. Samuelsson B, Morgenstern R, Jakobsson PJ (2007) Pharmacol Rev 59:207–224
3. Wang MT, Honn KV, Nie D (2007) Cancer Metastasis Rev 26:525–534
4. Schuligoi R et al (2010) Pharmacology 85:372–382
5. Jones RL, Giembycz MA, Woodward DF (2009) Br J Pharmacol 158:104–145
6. Matsuoka T, Narumiya S (2007) Sci World J 7:1329–1347
7. Hirai H et al (2001) J Exp Med 193:255–261
8. Hata AN, Breyer RM (2004) Pharmacol Ther 103:147–166
9. Kedzie KM, Donello JE, Krauss HA, Regan JW, Gil DW (1998) Mol Pharmacol 54:584–590
10. Chang C, Negishi M, Nishigaki N, Ichikawa A (1997) Biochem J 322:597–601
11. Stitham J, Stojanovic A, Merenick BL, O'Hara KA, Hwa J (2002) J Biol Chem 278:4250–4257
12. Funk CD, Furci L, Moran N, Fitzgerald GA (1993) Mol Pharmacol 44:934–939
13. Neuschäfer-Rube F, Engemaier E, Koch S, Böer U, Püschel GP (2003) Biochem J 371:443–449
14. Li Y et al (2007) J Am Chem Soc 129:10720–10731
15. Rosenbaum DM, Rasmussen SG, Kobilka BK (2009) Nature 459:356–363
16. Scheer A, Fanelli F, Costa T, De Benedetti PG, Cotecchia S (1996) EMBO J 15:3566–3578
17. Wess J (1998) Pharmacol Ther 80:231–264
18. Ballesteros J, Palczewski K (2001) Curr Opin Drug Discov Devel 4:561–574
19. Rosenkilde MM, Kledal TN, Schwartz TW (2005) Mol Pharmacol 68:11–19
20. Lu ZL, Curtis CA, Jones PG, Pavia J, Hulme EC (1997) Mol Pharmacol 51:234–241
21. Altschul SF, Madden TL, Schäffer AA, Zhang J, Zhang Z, Miller W, Lipman DJ (1997) Nucleic Acids Res 25:3389–3402
22. Ballesteros JA, Weinstein H (1995) Methods Neurosci 25:366–428
23. Katoh K, Misawa K, Kuma K, Miyata T (2002) Nucleic Acids Res 30:3059–3066
24. Katoh K, Toh H (2008) Brief Bioinform 9:286–298
25. Saitou N, Nei M (1987) Mol Biol Evol 4:406–425
26. Felsenstein J (1996) Methods Enzymol 266:418–427
27. Jones DT, Taylor WR, Thornton JM (1992) Comput Appl Biosci 8:275–282
28. Felsenstein J (1985) Evolution 39:783–791
29. Felsenstein J (1993) PHYLIP (phylogeny inference package), version 3.5c. University of Washington, Seattle
30. Adachi J, Hasegawa M (1996) MOLPHY (programs for molecular phylogenetics), version 2.3b3. Institute of Statistical Mathematics, Tokyo
31. Halgren TA (1996) J Comput Chem 17:490–519
32. Labute P (2008) J Comput Chem 29:1693–1698
33. Wiederstein M, Sippl MJ (2007) Nucleic Acids Res 35:W407–W410
34. Sippl MJ (1993) Proteins 17:355–362
35. Goto J, Kataoka R (2008) J Chem Inf Model 48:583–590
36. Bowers KJ, Chow E, Xu H, Dror RO, Eastwood MP, Gregersen BA, Klepeis JL, Kolossvary I, Moraes MA, Sacerdoti FD, Salmon JK, Shan Y, Shaw DE (2006) In: Proceedings of the ACM/IEEE conference on Supercomputing, Tampa, November 11-17, ACM New York, USA. doi:10.1145/1188455.1188544
37. Banks JL, Beard HS, Cao Y, Cho AE, Damm W, Farid B, Felts AK, Halgren TA, Mainz DT, Maple JR, Murphy R, Philipp DM, Repasky MP, Zhang LY, Berne BJ, Friesner RA, Gallicchio E, Levy RM (2005) J Comput Chem 26:1752–1780
38. Krautler V (2001) J Comput Chem 22:501–508
39. Darden T, York D, Pedersen L (1993) J Chem Phys 98:10089–10092
40. Lyne PD, Lamb M, Saeh JC (2006) J Med Chem 49:4805–4808
41. Toh H, Ichikawa A, Narumiya S (1995) FEBS Lett 361:17–21
42. Fritze O et al (2003) Proc Natl Acad Sci USA 100:2290–2295
43. Paila YD, Tiwari S, Chattopadhyay A (2008) Biochim Biophys Acta 1788:295–302
44. Dundas J, Ouyang Z, Tseng J, Binkowski A, Turpaz Y, Liang J (2006) Nucleic Acids Res 34:W116–W118
45. Jaakola V-P, Prilusky J, Sussman JL, Goldman A (2005) Protein Eng Des Sel 18:103–110
46. Kobayashi T, Ushikubi F, Narumiya S (2000) J Biol Chem 275:24294–24303
47. Tsuboi K, Sugimoto Y, Ichikawa A (2002) Prostaglandins Other Lipid Mediat 68–69:535–556
48. Vogel R, Mahalingam M, Lüdeke S, Huber T, Siebert F, Sakmar TP (2008) J Mol Biol 380:648–655
49. Rovati GE, Capra V, Neubig RR (2007) Mol Pharmacol 71:959–964
50. Pathe-Neuschäfer-Rube A, Neuschäfer-Rube F, Püschel GP (2005) Biochem J 388:317–324
51. Ambrosio M, Fanelli F, Brocchetti S, Raimondi F, Mauri M, Rovati GE, Capra V (2010) Cell Mol Life Sci 67:2979–2989
52. Tusnády GE, Dosztányi Z, Simon I (2005) Bioinformatics 21:1276–1277